(article starts on next page)

Performance studies on new 4″ photomultiplier types intended for IceCube-Gen2 optical modules

The IceCube-Gen2 Collaboration

(a complete list of authors can be found at the end of the proceedings)

E-mail: markus.dittmer@uni-muenster.de, alexander.kappes@uni-muenster.de

In the upcoming IceCube-Gen2 extension, the newly developed optical modules will include 4–inch PMTs. For this purpose, the manufacturers Hamamatsu and North Night Vision Technology have developed new PMT models to meet the requirements of the IceCube-Gen2 science case. The specifications include strict requirements on temporal resolution, detection efficiency, and dark noise. We summarize the efforts to measure these performance characteristics and show that both PMT models meet the performance specifications set by IceCube-Gen2. Prototype optical modules based on both PMT models will be deployed with the IceCube Upgrade in order to test them in situ and help decide on a vendor for the Gen2 extension.

Corresponding authors: Markus Dittmer[1][*], Alexander Kappes[1]

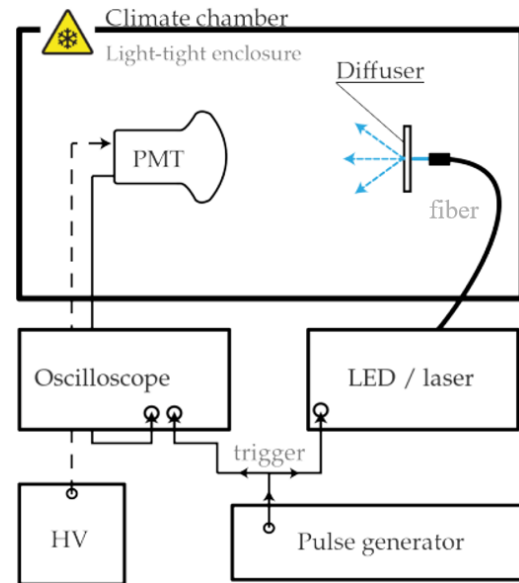[1] *University of Muenster*

[*] Presenter

1. Introduction

Photomultiplier-Tubes (PMTs) are the central component in Cherenkov telescopes such as BAIKAL-GVD [1], KM3NeT [2] and IceCube [3]. In the planned extension of IceCube-Gen2 [4], 4" PMTs will be integrated into the optical modules to be embedded in the Antarctic ice. Specifically for this purposes, the proposed PMT models R16293-01-Y001 (hereafter referred to as BB) and N2041 (hereafter referred to as PO) were developed by Hamamatsu Photonics K.K (HPK) and North Night Vision Technology (NNVT), respectively. This study focuses on the third and final iteration of the PMT development process, excluding the results from earlier prototyping stages. The performance of the utilized PMTs is a major contributor to the efficiency of the entire detector. Hence, strict requirements for various PMT characteristics have been set by the IceCube collaboration. The aim of the work described here is to verify that these specifications are met by conducting comparable measurements for both PMT models. This work is structured into temperature dependent measurements (Section 2), the PMT quantum efficiency (Section 3) and homogeneity studies (Section 4).

2. Temperature dependence

Since the optical modules of IceCube-Gen2 will be embedded in ice at different depths, with ambient temperatures ranging from $-8\,°C$ to $-40\,°C$ [6], it is crucial to examine the low temperature performance of the PMTs and its temperature dependency.

The measurements of this section were conducted using the setup depicted in Figure 1. It consists of a PMT illuminated by a LED at 385nm [7] through a fiber equipped with a diffuser which is placed inside a light-tight enclosure. The enclosure is further housed inside a climate chamber which is ramped in $10\,°C$ steps from $-50\,°C$ – $20\,°C$ with the measurements being performed for several hours at each temperature. The PMT response is captured by an oscilloscope and the maximum amplitude, time of this amplitude and charge within a specified window are recorded for each waveform. For a more

Figure 1: Experimental setup for the measurement of PMT pulse parameters. Taken from [5].

comprehensive understanding of the data acquisition, the reader is referred to [5, pp. 50-52]. With this setup, three different measurements were conducted for three Hamamatsu (BB9780, BB9786, BB9789) and three NNVT PMTs (PO4049, PO4052 PO4068) PMTs.

2.1 Gain calibration

The first measurement with this setup aims at determining the supply voltage for which an amplification of $5 \cdot 10^6$ is achieved. This amplification level is referred to as *nominal gain* and the corresponding supply voltage (dynode voltage ratio as recommended by the manufacturer) is known
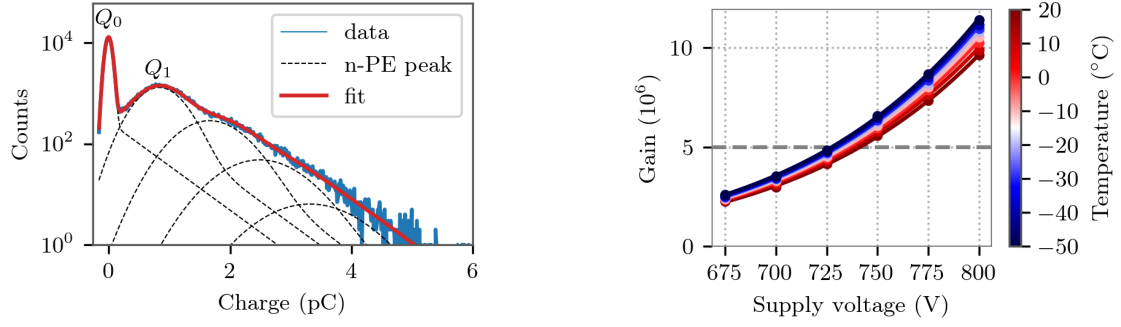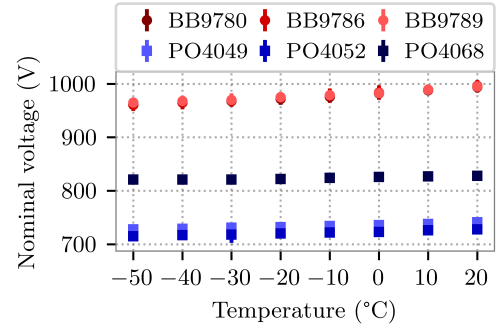
Figure 2: Example of SPE fit and gain curve for PO4049. The SPE fit of the charge histogram (left) provides the nominal gain, which represents one data point in the right plot. For each temperature, the nominal voltage (intersection with the gray line) is obtained.

as *nominal voltage*. For this, the supply voltage is varied at each temperature. The charge spectrum measured for a given voltage is fit by the Single Photoelectron (SPE) formula as described in [5, p. 45]. An example of the SPE fit is shown in Figure 2 (left).

From this fit, the gain can be obtained from the charge of a single photoelectron (Q_1/e) amongst other parameters. The nominal voltage for each temperature of each PMT is obtained by fitting a power law of the form cV^β [8, p. 206] which is shown in Figure 2 (right) whereas the corresponding nominal voltages for all PMTs are presented in Figure 3.

Decreasing the temperature by $\Delta T = 70\,°C$ results in an average gain increase of $(29.1 \pm 0.4)\,\%$ for Hamamatsu and $(13.6 \pm 0.3)\,\%$ for NNVT PMTs. This temperature dependence of the gain is most likely attributed to an increase of the secondary emission coefficient of the dynodes. The obtained nomi-

Figure 3: Nominal voltages plotted against operation temperature. NNVT PMTs are plotted in red and Hamamatsu PMTs in blue colors.

nal voltages are set in the subsequent measurements. Furthermore, it is observed that the Hamamatsu PMTs exhibit a smaller spread in nominal voltage compared to the NNVT PMTs which on the other hand need a lower supply voltage to achieve the same gain. Although the sample size within this study is limited, manufacturer data of large production batches support this claim.

2.2 Dark rate

The dark rate refers to the intrinsic background noise characterized by counting pulse rates in the absence of any illumination. Since background pulses appear randomly in time, long waveforms of 1 ms length were measured. From the number of pulses present in a given waveform one can calculate the dark rate which is done for more than 10^7 waveforms for each temperature step. To avoid triggering on baseline noise, a threshold of $3\,mV$ ($\sim 0.47\,PE$) was set. Consequently, low amplitude pulses are rejected. Since the charge is recorded and the nominal gain is known one can express this threshold in units of PE (charge/Q_1) which is shown in Figure 4 (left).
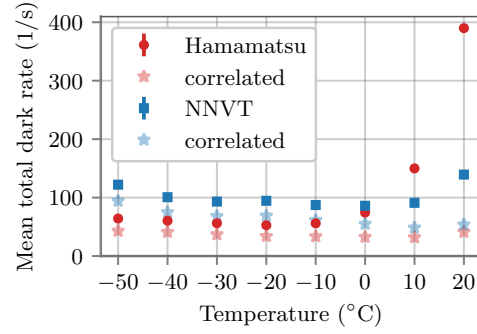
3
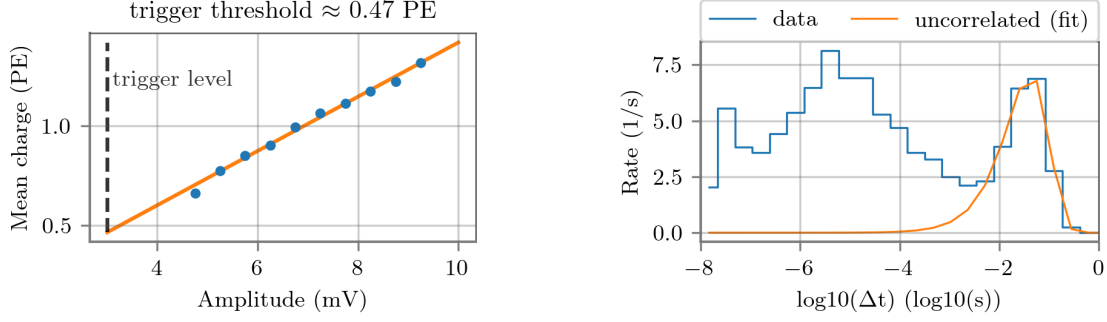
Figure 4: Additional evaluation for dark rates: (left) Binned amplitudes with the corresponding charge in units of PE where the trigger level in units of PE is obtained via a linear fit. (right) Fitting a Poissonian distribution onto the uncorrelated peak to classify noise contributions.

In addition to this amplitude threshold, a charge cut of 0.2 PE is set to further reject baseline noise. Note that a threshold–free measurement will produce higher dark rates than shown here.

A histogram based on the time difference between two successive pulses is shown in Figure 4 (right) where one can distinguish between correlated pulses caused by scintillation induced by radioactive decays in the glass bulb, and uncorrelated pulses, random pulses fitted by an exponential decay. For a more in–depth description, the reader is referred to [5, pp. 108-112].

Figure 5 displays the mean total dark rate of all PMTs from both vendors. Hamamatsu PMTs exhibit somewhat lower dark rates than NNVT PMTs at temperatures below 0 °C. This difference is attributed to the reduced presence of correlated noise in Hama-

Figure 5: Mean dark rates of both vendors plotted against temperature.

matsu PMTs, indicating less scintillation induced by radioactive decays from the enveloping glass bulb. However, at temperatures above 0 °C, the dark rates of Hamamatsu PMT increase significantly due to thermionic emission.

2.3 Timing resolution

To determine the timing characteristics, low light illumination (pulse occupancy less than 10%; <5 % multi-PE pulses) is used such that mostly SPE pulses contribute – otherwise the characteristics would yield different values in case multiple photons are detected simultaneously. The timing resolution, known as Transit Time Spread (TTS), is calculated from 10-µs-long waveforms.

For the TTS analysis, the relative pulse times with respect to the light source trigger are plotted in a histogram as shown in Figure 6 (left). The distribution of the histogram deviates from a Gaussian shape, particularly in the right *tail* region which is a consequence of full photocathode illumination in conjunction with the asymmetric curvature of the first dynode. While this is observed for all PMTs it is more pronounced in the models studied in this work. Hence, instead of fitting a Gaussian
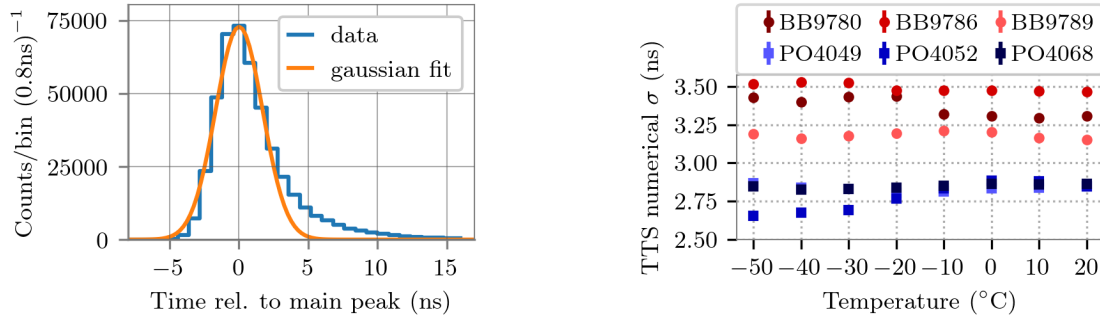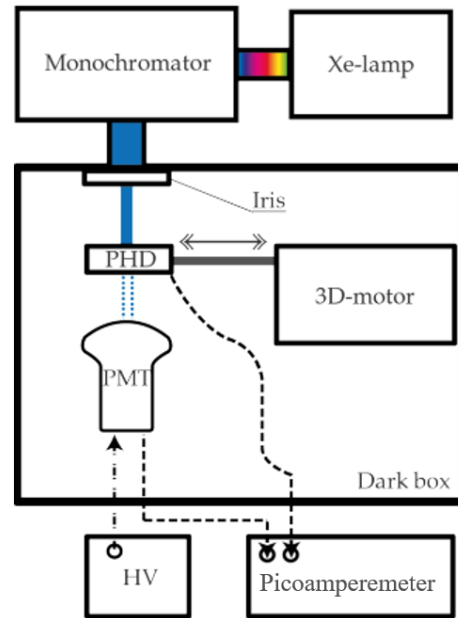
Figure 6: Evaluation for the TTS: (left) Binned arrival times, with the orange line indicating a Gaussian fit around the peak of the distribution and the blue line representing the data. (right) Comparison of the numerically calculated TTS plotted against temperature for each PMT.

distribution to the peak, the numerical standard deviation of the entire main peak distribution (-8 ns, 17 ns) is used (Figure 6 (right)). Overall, NNVT PMTs feature on average about (18.6 ± 0.1) % better time resolution compared to Hamamatsu PMTs. PMT BB9780 shows an increase of 3.5 % in TTS towards lower temperatures whilst PO4052 demonstrates an 8 % decrease. The other PMTs perform essentially constant (<1.5 % relative deviations). Though statistics is low Hamamatsu PMTs tend to have stronger variations in TTS, with comparatively twice the overall standard deviation.
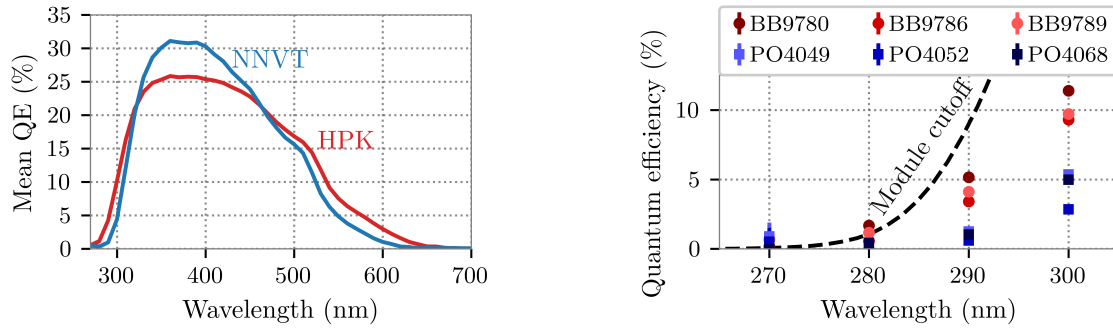
3. Quantum efficiency

The quantum efficiency (QE) is a crucial PMT characteristic. It represents the probability that a photoelectron is emitted by a photon striking the photocathode, and is wavelength dependent. For this, the setup shown in Figure 7 is used. The wavelength λ of high intensity light (emitted from a Xenon lamp) is selected by a monochromator in the range of 250 nm – 700 nm in increments of 10 nm. The beam is directed either to a calibrated photodiode (PHD in Figure 7) or a PMT. The PMT is attached to a base that shortcuts all dynodes, allowing collection of each photoelectron striking the multiplier system without multiplication. Since the beam is divergent, its spot size on the PMT can be adjusted to illuminate the entire photocathode by positioning the PMT further from the iris. The respective current I as well as the dark current DC are measured using a picoamperemeter. The quantum efficiency of the PMT is calculated using the equation

Figure 7: Experimental setup to measure the quantum efficiency. Taken from [5].

$$QE(\lambda) = \frac{I_{\text{PMT}}(\lambda) - DC_{\text{PMT}}}{I_{\text{Diode}}(\lambda) - DC_{\text{Diode}}} \cdot QE_{\text{Diode}}(\lambda).$$

Figure 8: Quantum efficiency for the entire spectral range (left) and near the module cutoff (right).

The results are shown in Figure 8. NNVT PMTs feature a higher maximum quantum efficiency at wavelengths around 360 nm ((31.1 ± 0.1)%) than Hamamatsu PMTs ((25.8 ± 0.1)%) which exhibit a slightly broader spectrum. Both PMT models feature a similar cutoff at around 270 nm since both PMT corpora consist of borosilicate glass. The same holds true for the pressure vessel of IceCube-Gen2s optical module as indicated by the black line in the right plot where a comparable PMT quantum efficiency is desired. Hamamatsu PMTs tend to show slightly higher quantum efficiencies near this cutoff which may be attributed to thinner glass in front of the photocathode area.

4. Homogeneity scan

Depending on the incident position of the photon on the photocathode, the aforementioned characteristics may change due to different path lengths of photoelectrons inside of a PMT.

Instead of using diffuse illumination, light from a collimated fiber is used to scan the photocathode surface (Figure 9). The PMT is located inside a Helmholtz-cube which is set to compensate Earth's magnetic field, nullifying its influence on the measurements, whereas the data acquisition is analogous to Section 2. For additional information, the reader is referred to [9].
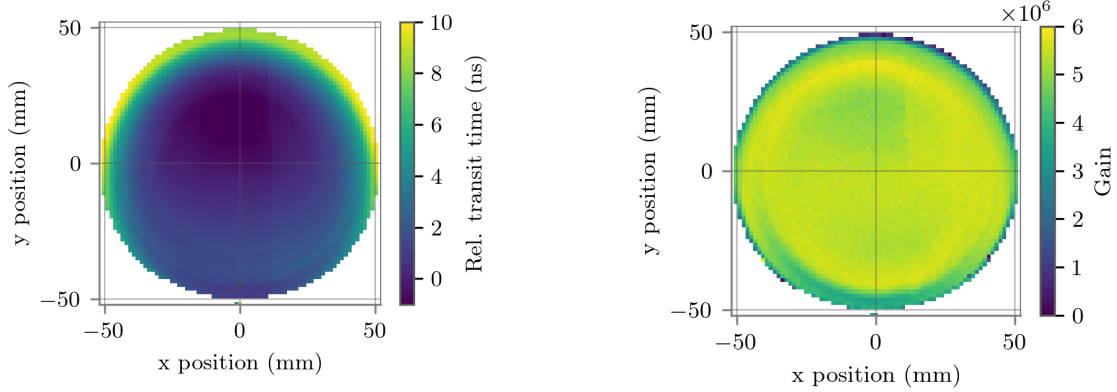
In the following, the center region is defined for the area with $r < 30$ mm and the edge region for the area with $r > 45$ mm. The resulting scan of the

Figure 9: Experimental setup to scan the photocathode. Taken from [9].

transit time relative to the center region and the absolute gain is shown in Figure 10. It is apparent that the performance deteriorates towards the edges which is averaged over in the diffuse light measurements as presented in Section 2. The asymmetric distribution of the transit time values arises from the first dynode being curved in the positive y-direction in this representation.

While the gain values demonstrate relatively homogeneous behavior across the radial distance, the transit time values exhibit a noticeable slope along the y-direction. In order to compare both PMT models, instead of heatmaps as presented in Figure 10, the results in Figure 11 are shown as scatter plots as a function of radial distance to the photocathode center.
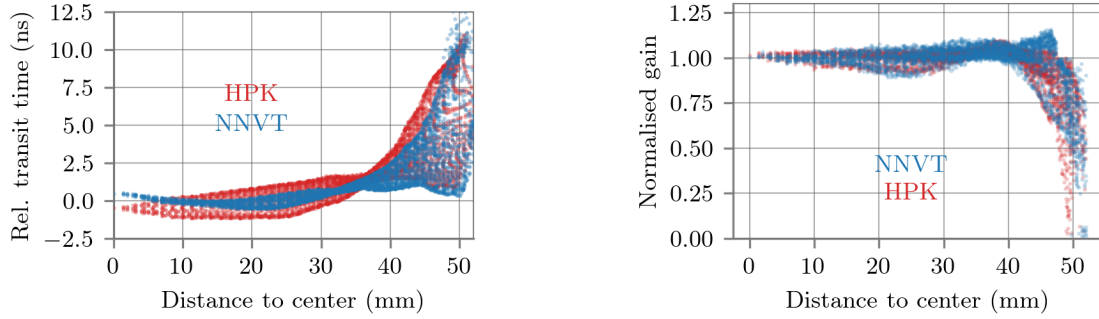
Figure 10: Entire data set for relative transit time (left) and absolute gain (right) for BB9786.

Figure 11: Comparison between both PMT models as a function of radial distance towards center. (left) Transit time relative to the center. (right) Gain normalised to the center.

Comparing both data sets, the mean and standard deviations for the overall transit time are (1.75 ± 2.48) ns for NNVT and (2.10 ± 2.66) ns for Hamamatsu PMTs whereas the edge regions exhibit values of (5.37 ± 3.46) ns and (5.93 ± 3.07) ns respectively, while NNVT PMTs show slightly higher maximum deviations but a more uniform distribution in the center. Thus, NNVT PMTs demonstrate a more uniform timing response in the center but worse towards the edges. Contrarily, regarding the gain, the standard deviations relative to the mean in the center are 3.7 % (NNVT) and 3.1 % (Hamamatsu), whereas at the edges, they are 20.5 % (NNVT) and 19.0 % (Hamamatsu). Smoothed curves reveal a drop of 20% in gain at approximately $0.93 \cdot r$ for both models and a slight increase in gain is observed around 40 mm. In both regards the investigated 4-inch PMTs exhibit similar performance and are within the expectations. However, it is important to note that only a single PMT from each vendor was measured.

5. Conclusion

Considering the importance of the PMTs' outer dimensions for module construction (refer to [10]), the performance requirements have a certain degree of flexibility. The metrics presented in this work are listed in Table 1, and both manufacturers fulfill the specifications set by the collaboration.

In summary, NNVT PMTs operate at lower nominal voltages and exhibit higher dark rates due to correlated noise, with larger PMT-to-PMT fluctuations compared to Hamamatsu PMTs. NNVT PMTs offer better timing resolution and higher quantum efficiency, though with a slightly higher cutoff. Whilst NNVT PMTs are slightly more homogeneous in the PMT center, the PMT response exhibits more variation towards the edges. Although this study had a limited sample size and more PMTs need to be measured, the results suggest that the tested 4-inch NNVT PMTs performed slightly better compared to Hamamatsu PMTs. To conclude, both vendors are viable options for the optical modules of IceCube-Gen2, which require production of over 160,000 PMTs.

Table 1: PMT requirements considered in this work. The TTS is defined as 8 ns (FWHM), and the values stated here represent the standard deviations of a Gaussian fit to the peak of the main peak timing histogram.

	Req.	BB9780	BB9786	BB9789	PO4049	PO4052	PO4052
Nominal Voltage (V)	< 1500	994	996	995	741	728	828
TTS (ns)	< 3.4	2.51	2.58	2.38	1.75	1.86	1.75
Max QE (%)	> 25	25.95	26.24	25.29	29.85	30.15	33.24

References

[1] **BAIKAL-GVD** Collaboration, A. D. Avrorin *et al. Bulletin of the Russian Academy of Sciences: Physics* **83** no. 8, (Aug., 2019) 921–922.

[2] **KM3Net** Collaboration, S. Adrián-Martínez *et al. Journal of Physics G: Nuclear and Particle Physics* **43** no. 8, (June, 2016) 084001.

[3] **IceCube** Collaboration, M. Aartsen *et al. Journal of Instrumentation* **12** no. 03, (Mar., 2017) P03012.

[4] **IceCube** Collaboration, M. G. Aartsen *et al. Journal of Physics G: Nuclear and Particle Physics* **48** no. 6, (Apr., 2021) 060501.

[5] M. Unland, *Development, simulation, and characterisation of a novel multi-PMT optical module for IceCube Upgrade with emphasis on detailed understanding of photomultiplier performance parameters*. PhD thesis, WWU Münster, 2023.

[6] P. B. Price *et al. Proceedings of the National Academy of Sciences* **99** no. 12, (June, 2002) 7844–7847.

[7] M. Rongen and M. Schaufel *Journal of Instrumentation* **13** no. 06, (June, 2018) P06002.

[8] A. G. Wright, *The Photomultiplier Handbook*. Oxford University Press, Aug., 2017. https://doi.org/10.1093/oso/9780199565092.001.0001.

[9] M. Unland *et al. journal of Instrumentation* **16** (2021) P11038.

[10] **IceCube** Collaboration, Y. Makino *PoS* **ICRC2023** (these proceedings) 979.

Full Author List: IceCube-Gen2 Collaboration

R. Abbasi[17], M. Ackermann[76], J. Adams[22], S. K. Agarwalla[47, 77], J. A. Aguilar[12], M. Ahlers[26], J.M. Alameddine[27], N. M. Amin[53], K. Andeen[50], G. Anton[30], C. Argüelles[14], Y. Ashida[64], S. Athanasiadou[76], J. Audehm[1], S. N. Axani[53], X. Bai[61], A. Balagopal V.[47], M. Baricevic[47], S. W. Barwick[34], V. Basu[47], R. Bay[8], J. Becker Tjus[11, 78], J. Beise[74], C. Bellenghi[31], C. Benning[1], S. BenZvi[63], D. Berley[23], E. Bernardini[59], D. Z. Besson[40], A. Bishop[47], E. Blaufuss[23], S. Blot[76], F. Bohmer[31], F. Bontempo[35], J. Y. Book[14], J. Borowka[1], C. Boscolo Meneguolo[59], S. Böser[48], O. Botner[74], J. Böttcher[1], S. Bouma[30], E. Bourbeau[26], J. Braun[47], B. Brinson[6], J. Brostean-Kaiser[76], R. T. Burley[2], R. S. Busse[52], D. Butterfield[47], M. A. Campana[60], K. Carloni[14], E. G. Carnie-Bronca[2], M. Cataldo[30], S. Chattopadhyay[47, 77], N. Chau[12], C. Chen[6], Z. Chen[66], D. Chirkin[47], S. Choi[67], B. A. Clark[23], R. Clark[42], L. Classen[52], A. Coleman[74], G. H. Collin[15], J. M. Conrad[15], D. F. Cowen[71, 72], B. Dasgupta[51], P. Dave[6], C. Deaconu[20, 21], C. De Clercq[13], S. De Kockere[13], J. J. DeLaunay[70], D. Delgado[14], S. Deng[1], K. Deoskar[65], A. Desai[47], P. Desiati[47], K. D. de Vries[13], G. de Wasseige[44], T. DeYoung[28], A. Diaz[15], J. C. Díaz-Vélez[47], M. Dittmer[52], A. Domi[30], H. Dujmovic[47], M. A. DuVernois[47], T. Ehrhardt[48], P. Eller[31], E. Ellinger[75], S. El Mentawi[1], D. Elsässer[27], R. Engel[35, 36], H. Erpenbeck[47], J. Evans[23], J. J. Evans[49], P. A. Evenson[53], K. L. Fan[23], K. Fang[47], K. Farrag[43], K. Farrag[16], A. R. Fazely[7], A. Fedynitch[68], N. Feigl[10], S. Fiedlschuster[30], C. Finley[65], L. Fischer[76], B. Flaggs[53], D. Fox[71], A. Franckowiak[11], A. Fritz[48], T. Fujii[57], P. Fürst[1], J. Gallagher[46], E. Ganster[1], A. Garcia[14], L. Gerhardt[9], R. Gernhaeuser[31], A. Ghadimi[70], P. Giri[41], C. Glaser[74], T. Glauch[31], T. Glüsenkamp[30, 74], N. Goehlke[36], S. Goswami[70], D. Grant[28], S. J. Gray[23], O. Gries[1], S. Griffin[47], S. Griswold[63], D. Guevel[47], C. Günther[1], P. Gutjahr[27], C. Haack[30], T. Haji Azim[1], A. Hallgren[74], R. Halliday[28], S. Hallmann[76], L. Halve[1], F. Halzen[47], H. Hamdaoui[66], M. Ha Minh[31], K. Hanson[47], J. Hardin[15], A. A. Harnisch[28], P. Hatch[37], J. Haugen[47], A. Haungs[35], D. Heinen[1], K. Helbing[75], J. Hellrung[11], B. Hendricks[72, 73], F. Henningsen[31], J. Henrichs[76], L. Heuermann[1], N. Heyer[74], S. Hickford[75], A. Hidvegi[65], J. Hignight[29], C. Hill[16], G. C. Hill[2], K. D. Hoffman[23], B. Hoffmann[36], K. Holzapfel[31], S. Hori[47], K. Hoshina[47, 79], W. Hou[35], T. Huber[35], T. Huege[35], K. Hughes[19, 21], K. Hultqvist[65], M. Hünnefeld[27], R. Hussain[47], K. Hymon[27], S. In[67], A. Ishihara[16], M. Jacquart[47], O. Janik[1], M. Jansson[65], G. S. Japaridze[5], M. Jeong[67], M. Jin[14], B. J. P. Jones[4], O. Kalekin[30], D. Kang[35], W. Kang[67], X. Kang[60], A. Kappes[52], D. Kappesser[48], L. Kardum[27], T. Karg[76], M. Karl[31], A. Karle[47], T. Katori[42], U. Katz[30], M. Kauer[47], J. L. Kelley[47], A. Khatee Zathul[47], A. Kheirandish[38, 39], J. Kiryluk[66], S. R. Klein[8, 9], T. Kobayashi[57], A. Kochocki[28], H. Kolanoski[10], T. Kontrimas[31], L. Köpke[48], C. Kopper[30], D. J. Koskinen[26], P. Koundal[35], M. Kovacevich[60], M. Kowalski[10, 76], T. Kozynets[26], C. B. Krauss[29], I. Kravchenko[41], J. Krishnamoorthi[47, 77], E. Krupczak[28], A. Kumar[76], E. Kun[11], N. Kurahashi[60], N. Lad[76], C. Lagunas Gualda[76], M. J. Larson[23], S. Latseva[1], F. Lauber[75], J. P. Lazar[14, 47], J. W. Lee[67], K. Leonard DeHolton[72], A. Leszczyńska[53], M. Lincetto[11], Q. R. Liu[47], M. Liubarska[29], M. Lohan[51], E. Lohfink[48], J. LoSecco[56], C. Love[60], C. J. Lozano Mariscal[52], L. Lu[47], F. Lucarelli[32], Y. Lyu[8, 9], J. Madsen[47], K. B. M. Mahn[28], Y. Makino[47], S. Mancina[47, 59], S. Mandalia[43], W. Marie Sainte[47], I. C. Mariş[12], S. Marka[55], Z. Marka[55], M. Marsee[70], I. Martinez-Soler[14], R. Maruyama[54], F. Mayhew[28], T. McElroy[29], F. McNally[45], J. V. Mead[26], K. Meagher[47], S. Mechbal[76], A. Medina[25], M. Meier[16], Y. Merckx[13], L. Merten[11], Z. Meyers[76], J. Micallef[28], M. Mikhailova[40], J. Mitchell[7], T. Montaruli[32], R. W. Moore[29], Y. Morii[16], R. Morse[47], M. Moulai[47], T. Mukherjee[35], R. Naab[76], R. Nagai[16], M. Nakos[47], A. Narayan[51], U. Naumann[75], J. Necker[76], A. Negi[4], A. Nelles[30, 76], M. Neumann[52], H. Niederhausen[28], M. U. Nisa[28], A. Noell[1], A. Novikov[53], S. C. Nowicki[28], A. Nozdrina[40], E. Oberla[20, 21], A. Obertacke Pollmann[16], V. O'Dell[47], M. Oehler[35], B. Oeyen[33], A. Olivas[23], R. Ørsøe[31], J. Osborn[47], E. O'Sullivan[74], L. Papp[31], N. Park[37], G. K. Parker[4], E. N. Paudel[53], L. Paul[50, 61], C. Pérez de los Heros[74], T. C. Petersen[26], J. Peterson[47], S. Philippen[1], S. Pieper[75], J. L. Pinfold[29], A. Pizzuto[47], I. Plaisier[76], M. Plum[61], A. Pontén[74], Y. Popovych[48], M. Prado Rodriguez[47], B. Pries[28], R. Procter-Murphy[23], G. T. Przybylski[9], L. Pyras[76], J. Rack-Helleis[48], M. Rameez[51], K. Rawlins[3], Z. Rechav[47], A. Rehman[53], P. Reichherzer[11], G. Renzi[12], E. Resconi[31], S. Reusch[76], W. Rhode[27], B. Riedel[47], M. Riegel[35], A. Rifaie[1], E. J. Roberts[2], S. Robertson[8, 9], S. Rodan[67], G. Roellinghoff[67], M. Rongen[30], C. Rott[64, 67], T. Ruhe[27], D. Ryckbosch[33], I. Safa[14, 47], J. Saffer[36], D. Salazar-Gallegos[28], P. Sampathkumar[35], S. E. Sanchez Herrera[28], A. Sandrock[75], P. Sandstrom[47], M. Santander[70], S. Sarkar[29], S. Sarkar[58], J. Savelberg[1], P. Savina[47], M. Schaufel[1], H. Schieler[35], S. Schindler[30], L. Schlickmann[1], B. Schlüter[52], F. Schlüter[12], N. Schmeisser[75], T. Schmidt[23], J. Schneider[30], F. G. Schröder[35, 53], L. Schumacher[30], G. Schwefer[1], S. Sclafani[23], D. Seckel[53], M. Seikh[40], S. Seunarine[62], M. H. Shaevitz[55], R. Shah[60], A. Sharma[74], S. Shefali[36], N. Shimizu[16], M. Silva[47], B. Skrzypek[14], D. Smith[19, 21], B. Smithers[4], R. Snihur[47], J. Soedingrekso[27], A. Søgaard[26], D. Soldin[36], P. Soldin[1], G. Sommani[11], D. Southall[19, 21], C. Spannfellner[31], G. M. Spiczak[62], C. Spiering[76], M. Stamatikos[25], T. Stanev[53], T. Stezelberger[9], J. Stoffels[13], T. Stürwald[75], T. Stuttard[26], G. W. Sullivan[23], I. Taboada[6], A. Taketa[69], H. K. M. Tanaka[69], S. Ter-Antonyan[7], M. Thiesmeyer[1], W. G. Thompson[14], J. Thwaites[47], S. Tilav[53], K. Tollefson[28], C. Tönnis[67], J. Torres[24, 25], S. Toscano[12], D. Tosi[47], A. Trettin[76], Y. Tsunesada[57], C. F. Tung[6], R. Turcotte[35], J. P. Twagirayezu[28], B. Ty[47], M. A. Unland Elorrieta[52], A. K. Upadhyay[47, 77], K. Upshaw[7], N. Valtonen-Mattila[74], J. Vandenbroucke[47], N. van Eijndhoven[13], D. Vannerom[15], J. van Santen[76], J. Vara[52], D. Veberic[35], J. Veitch-Michaelis[47], M. Venugopal[35], S. Verpoest[53], A. Vieregg[18, 19, 20, 21], A. Vijai[23], C. Walck[65], C. Weaver[28], P. Weigel[15], A. Weindl[35], J. Weldert[72], C. Welling[21], C. Wendt[47], J. Werthebach[27], M. Weyrauch[35], N. Whitehorn[28], C. H. Wiebusch[1], N. Willey[28], D. R. Williams[70], S. Wissel[71, 72, 73], L. Witthaus[27], A. Wolf[1], M. Wolf[31], G. Wörner[35], G. Wrede[30], S. Wren[49], X. W. Xu[7], J. P. Yanez[29], E. Yildizci[47], S. Yoshida[16], R. Young[40], F. Yu[14], S. Yu[28], T. Yuan[47], Z. Zhang[66], P. Zhelnin[14], S. Zierke[1], M. Zimmerman[47]

[1] III. Physikalisches Institut, RWTH Aachen University, D-52056 Aachen, Germany
[2] Department of Physics, University of Adelaide, Adelaide, 5005, Australia
[3] Dept. of Physics and Astronomy, University of Alaska Anchorage, 3211 Providence Dr., Anchorage, AK 99508, USA
[4] Dept. of Physics, University of Texas at Arlington, 502 Yates St., Science Hall Rm 108, Box 19059, Arlington, TX 76019, USA
[5] CTSPS, Clark-Atlanta University, Atlanta, GA 30314, USA
[6] School of Physics and Center for Relativistic Astrophysics, Georgia Institute of Technology, Atlanta, GA 30332, USA

[7] Dept. of Physics, Southern University, Baton Rouge, LA 70813, USA

[8] Dept. of Physics, University of California, Berkeley, CA 94720, USA

[9] Lawrence Berkeley National Laboratory, Berkeley, CA 94720, USA

[10] Institut für Physik, Humboldt-Universität zu Berlin, D-12489 Berlin, Germany

[11] Fakultät für Physik & Astronomie, Ruhr-Universität Bochum, D-44780 Bochum, Germany

[12] Université Libre de Bruxelles, Science Faculty CP230, B-1050 Brussels, Belgium

[13] Vrije Universiteit Brussel (VUB), Dienst ELEM, B-1050 Brussels, Belgium

[14] Department of Physics and Laboratory for Particle Physics and Cosmology, Harvard University, Cambridge, MA 02138, USA

[15] Dept. of Physics, Massachusetts Institute of Technology, Cambridge, MA 02139, USA

[16] Dept. of Physics and The International Center for Hadron Astrophysics, Chiba University, Chiba 263-8522, Japan

[17] Department of Physics, Loyola University Chicago, Chicago, IL 60660, USA

[18] Dept. of Astronomy and Astrophysics, University of Chicago, Chicago, IL 60637, USA

[19] Dept. of Physics, University of Chicago, Chicago, IL 60637, USA

[20] Enrico Fermi Institute, University of Chicago, Chicago, IL 60637, USA

[21] Kavli Institute for Cosmological Physics, University of Chicago, Chicago, IL 60637, USA

[22] Dept. of Physics and Astronomy, University of Canterbury, Private Bag 4800, Christchurch, New Zeland

[23] Dept. of Physics, University of Maryland, College Park, MD 20742, USA

[24] Dept. of Astronomy, Ohio State University, Columbus, OH 43210, USA

[25] Dept. of Physics and Center for Cosmology and Astro-Particle Physics, Ohio State University, Columbus, OH 43210, USA

[26] Niels Bohr Institute, University of Copenhagen, DK-2100 Copenhagen, Denmark

[27] Dept. of Physics, TU Dortmund University, D-44221 Dortmund, Germany

[28] Dept. of Physics and Astronomy, Michigan State University, East Lansing, MI 48824, USA

[29] Dept. of Physics, University of Alberta, Edmonton, Alberta, Canada T6G 2E1

[30] Erlangen Centre for Astroparticle Physics, Friedrich-Alexander-Universität Erlangen-Nürnberg, D-91058 Erlangen, Germany

[31] Technical University of Munich, TUM School of Natural Sciences, Department of Physics, D-85748 Garching bei München, Germany

[32] Département de physique nucléaire et corpusculaire, Université de Genève, CH-1211 Genève, Switzerland

[33] Dept. of Physics and Astronomy, University of Gent, B-9000 Gent, Belgium

[34] Dept. of Physics and Astronomy, University of California, Irvine, CA 92697, USA

[35] Karlsruhe Institute of Technology, Institute for Astroparticle Physics, D-76021 Karlsruhe, Germany

[36] Karlsruhe Institute of Technology, Institute of Experimental Particle Physics, D-76021 Karlsruhe, Germany

[37] Dept. of Physics, Engineering Physics, and Astronomy, Queen's University, Kingston, ON K7L 3N6, Canada

[38] Department of Physics & Astronomy, University of Nevada, Las Vegas, NV, 89154, USA

[39] Nevada Center for Astrophysics, University of Nevada, Las Vegas, NV 89154, USA

[40] Dept. of Physics and Astronomy, University of Kansas, Lawrence, KS 66045, USA

[41] Dept. of Physics and Astronomy, University of Nebraska–Lincoln, Lincoln, Nebraska 68588, USA

[42] Dept. of Physics, King's College London, London WC2R 2LS, United Kingdom

[43] School of Physics and Astronomy, Queen Mary University of London, London E1 4NS, United Kingdom

[44] Centre for Cosmology, Particle Physics and Phenomenology - CP3, Université catholique de Louvain, Louvain-la-Neuve, Belgium

[45] Department of Physics, Mercer University, Macon, GA 31207-0001, USA

[46] Dept. of Astronomy, University of Wisconsin–Madison, Madison, WI 53706, USA

[47] Dept. of Physics and Wisconsin IceCube Particle Astrophysics Center, University of Wisconsin–Madison, Madison, WI 53706, USA

[48] Institute of Physics, University of Mainz, Staudinger Weg 7, D-55099 Mainz, Germany

[49] School of Physics and Astronomy, The University of Manchester, Oxford Road, Manchester, M13 9PL, United Kingdom

[50] Department of Physics, Marquette University, Milwaukee, WI, 53201, USA

[51] Dept. of High Energy Physics, Tata Institute of Fundamental Research, Colaba, Mumbai 400 005, India

[52] Institut für Kernphysik, Westfälische Wilhelms-Universität Münster, D-48149 Münster, Germany

[53] Bartol Research Institute and Dept. of Physics and Astronomy, University of Delaware, Newark, DE 19716, USA

[54] Dept. of Physics, Yale University, New Haven, CT 06520, USA

[55] Columbia Astrophysics and Nevis Laboratories, Columbia University, New York, NY 10027, USA

[56] Dept. of Physics, University of Notre Dame du Lac, 225 Nieuwland Science Hall, Notre Dame, IN 46556-5670, USA

[57] Graduate School of Science and NITEP, Osaka Metropolitan University, Osaka 558-8585, Japan

[58] Dept. of Physics, University of Oxford, Parks Road, Oxford OX1 3PU, United Kingdom

[59] Dipartimento di Fisica e Astronomia Galileo Galilei, Università Degli Studi di Padova, 35122 Padova PD, Italy

[60] Dept. of Physics, Drexel University, 3141 Chestnut Street, Philadelphia, PA 19104, USA

[61] Physics Department, South Dakota School of Mines and Technology, Rapid City, SD 57701, USA

[62] Dept. of Physics, University of Wisconsin, River Falls, WI 54022, USA

[63] Dept. of Physics and Astronomy, University of Rochester, Rochester, NY 14627, USA

[64] Department of Physics and Astronomy, University of Utah, Salt Lake City, UT 84112, USA

[65] Oskar Klein Centre and Dept. of Physics, Stockholm University, SE-10691 Stockholm, Sweden

[66] Dept. of Physics and Astronomy, Stony Brook University, Stony Brook, NY 11794-3800, USA

[67] Dept. of Physics, Sungkyunkwan University, Suwon 16419, Korea

[68] Institute of Physics, Academia Sinica, Taipei, 11529, Taiwan

[69] Earthquake Research Institute, University of Tokyo, Bunkyo, Tokyo 113-0032, Japan

[70] Dept. of Physics and Astronomy, University of Alabama, Tuscaloosa, AL 35487, USA

[71] Dept. of Astronomy and Astrophysics, Pennsylvania State University, University Park, PA 16802, USA

[72] Dept. of Physics, Pennsylvania State University, University Park, PA 16802, USA

[73] Institute of Gravitation and the Cosmos, Center for Multi-Messenger Astrophysics, Pennsylvania State University, University Park, PA 16802, USA

[74] Dept. of Physics and Astronomy, Uppsala University, Box 516, S-75120 Uppsala, Sweden

[75] Dept. of Physics, University of Wuppertal, D-42119 Wuppertal, Germany

[76] Deutsches Elektronen-Synchrotron DESY, Platanenallee 6, 15738 Zeuthen, Germany

[77] Institute of Physics, Sachivalaya Marg, Sainik School Post, Bhubaneswar 751005, India

[78] Department of Space, Earth and Environment, Chalmers University of Technology, 412 96 Gothenburg, Sweden

[79] Earthquake Research Institute, University of Tokyo, Bunkyo, Tokyo 113-0032, Japan